================================= README.TXT =================================

All Authors: F. Buchter, Z. Lodziana, A. Remhof, Ph. Mauron, O. Friedrichs, A. Borgschulte, A. Züttel, Y. Filinchuk, L. Palatinus

Title: Experimental charge density of LiBD4 from maximum entropy method

Description:
1.) The additional information contains a .tex file and twenty supplementary figures.

2) In cases where we refer to a figure or a table of the main manuscript in the EPAPS file, we explicitly mention it

3) In the title of the EPAPS file, we explicitly mention that this contains the Supplemental information.

Total No. of Files: 22

Filenames:
FigS1.jpg, FigS2.jpg, FigS3.jpg, FigS4.jpg, FigS5.jpg, FigS6.jpg, FigS7.jpg, FigS8.jpg, FigS9.jpg, FigS10.jpg, FigS11.jpg, FigS12.jpg, FigS13.jpg, FigS14.jpg, FigS15.jpg, FigS16.jpg, FigS17.jpg, FigS18.jpg, FigS19.jpg, FigS20.jpg, README.TXT, LIBD4_MEM_charge_density_support.tex

Filetypes: One text file (.tex), containing the also the figure captions and twenty figures as jpg-files.

Special Instructions:
The supplemental text is written using REVTEX and contains the figure captions as well as some tables. It may be treated as a "normal" manuscript. It has the same header as the main manuscript, however the title says "Supplemental Material"

Contact information:
Arndt Remhof
Empa -
Swiss Federal Laboratories for Materials Testing and Research
Hydrogen and Energy
Überlandstrasse 129
CH-8600 Dübendorf
Switzerland
Phone: 011+41-44-823-4369   FAX: 011+41-44-823-4022
Email: arndt.remhof@empa.ch

==

I. SUPPLEMENTAL MATERIAL

A. Rietveld refinements

TABLE I: Summary of refined parameters. Thomson-Cox-Hastings modified pseudo-Voigt profile functions were used to model the peak shape for both SR-XPD and NPD diffraction patterns. The background is modeled by a 12 refined coefficients Fourier-cosine series for the NPD data and an interpolation between fixed points for the SR-XPD data. Anisotropic strain and size broadening was used fo the SR-XPD data at 10 K. No soft restraints are applied. The refinements against the image plate data (combined with NPD data or not) are always performed against the three SR-XPD diffraction data collected at different detector-sample distances (150 mm, 200 mm, 300 mm).

Detector	X-HR	XN-HR	X-HR	XN-HR	X-IP	XN-IP
Temperature	10	10	90	90	90	90
Weight patterns NPD/SR-XPD	0	1/5	0	1/10	0	1/100
Structure refined param.	21	41	21	41	24	47
Profile refined param.*	15	21	15	22	14	19
Background points	51	63	51	63	175	187
Total refined param.	87	125	87	126	213	253

* Including scale factors, and zero shift

FIG. 1: SR-XPD diffraction pattern of the $LiBD_4$ at 10 K and result of the Rietveld refinement of the $LiBD_4$ structural model.

FIG. 2: NPD (Top) and SR-XPD (Bottom) diffraction pattern of the $LiBD_4$ at 10 K, and result of the combined Rietveld refinement of the $LiBD_4$ structural model. Excluded regions are, for diffraction peaks arising from the Al thermal shielding not completely removed by the radial collimator.

FIG. 3: SR-XPD diffraction pattern (high resolution powder diffractometer) of the $LiBD_4$ at 90 K and result of the Rietveld refinement of the $LiBD_4$ structural model.

FIG. 4: NPD (Top) and SR-XPD (Bottom) diffraction pattern (high resolution powder diffractometer) of the $LiBD_4$ at 90 K, and result of the combined Rietveld refinement of the $LiBD_4$ structural model.

FIG. 5: SR-XPD diffraction pattern (image plate detector powder diffractometer) of the $LiBD_4$ at 90 K and result of the Rietveld refinement of the $LiBD_4$ structural model. Sample-detector distances: 300mm (Top), 200mm (Middle), 300mm (Bottom).

FIG. 6: NPD (Top) and SR-XPD (Bottom) diffraction pattern (image plate detector powder diffractometer) of the $LiBD_4$ at 90 K, and result of the combined Rietveld refinement of the $LiBD_4$ structural model. Sample-detector distances: 300mm (Top), 200mm (Middle), 300mm (Bottom).

TABLE II: Refined structural parameters of the low-T phase of $LiBD_4$ at 10 K. Space group *Pnma* (No. 62), Z=4.

Site	Data‡-Setup§	x/a	y/b	z/c	U$_{iso}$ (Å^2)
Li/4c	X-HR	0.1587(6)	0.25	0.1135(6)	0.016(4)
	XN-HR	0.1577(9)	0.25	0.1136(12)	0.024(6)*
B/4c	X-HR	0.3043(4)	0.25	0.4292(5)	0.005(2)
	XN-HR	0.3041(5)	0.25	0.4302(6)	0.007(3)*
D1/4c	X-HR	0.8979(15)	0.25	0.935(3)	-0.003(3)†
	XN-HR	0.9059(12)	0.25	0.926(2)	0.019(5)*
D2/4c	X-HR	0.3949(21)	0.25	0.286(2)	-0.003(3)†
	XN-HR	0.3986(18)	0.25	0.2788(15)	0.025(6)*
D3/8d	X-HR	0.2104(15)	0.0400(21)	0.4294(15)	-0.003(3)†
	XN-HR	0.2033(9)	0.0289(12)	0.4287(12)	0.026(4)*

X-HR; a=7.11351(9) Å, b=4.40442(5) Å, c=6.67213(9) Å

XN-HR; a=7.11346(18) Å, b=4.4278(12) Å, c=6.6720(2) Å

* Equivalent isotropic thermal factor

† All D atoms are constrained to have the same displacement parameters

Small negative U$_{iso}$ within standard deviation are statistically undistiguishable from small positive values.

‡ Data used for the refinement; X: SR-XPD data; XN: combined SR-XPD/NPD data

§ HR: High resolution powder diffractometer

TABLE III: Refined structural parameters of the low-T phase of $LiBD_4$ at 90 K. Space group *Pnma* (No. 62), Z=4.

Site	Data[‡]-Setup[§]	x/a	y/b	z/c	U_{iso} (Å^2)
Li/4c	X-HR	0.15929(20)	0.25	0.1132(6)	0.0217(12)
	XN-HR	0.1591(12)	0.25	0.1131(12)	0.031(2)*
	X-IP	0.1577(12)	0.25	0.1142(12)	0.028(2)
	XN-IP	0.1578(15)	0.25	0.1150(15)	0.037(3)*
B/4c	X-HR	0.3040(4)	0.25	0.4292(5)	0.0092(7)
	XN-HR	0.3038(6)	0.25	0.4299(6)	0.0110(10)*
	X-IP	0.3056(9)	0.25	0.4282(9)	0.0139(7)
	XN-IP	0.3040(9)	0.25	0.4296(9)	0.0144(14)*
D1/4c	X-HR	0.8975(15)	0.25	0.937(3)	0.0008(10)[†]
	XN-HR	0.9034(14)	0.25	0.929(3)	0.0275(19)*
	X-IP	0.9002(27)	0.25	0.934(6)	0.007(2)[†]
	XN-IP	0.9038(21)	0.25	0.929(4)	0.027(3)*
D2/4c	X-HR	0.3944(21)	0.25	0.2861(24)	0.0008(10)[†]
	XN-HR	0.3991(18)	0.25	0.2797(18)	0.037(3)*
	X-IP	0.397(5)	0.25	0.278(5)	0.007(2)[†]
	XN-IP	0.399(3)	0.25	0.279(3)	0.036(5)*
D3/8d	X-HR	0.2090(15)	0.0404(21)	0.4302(15)	0.0008(10)[†]
	XN-HR	0.2019(9)	0.0327(12)	0.4284(12)	0.0375(13)*
	X-IP	0.205(3)	0.047(4)	0.434(4)	0.007(2)[†]
	XN-IP	0.2011(18)	0.0339(18)	0.4294(21)	0.037(2)*

X-HR; a=7.10621(9) Å, b=4.40627(4) Å, c=6.68275(9) Å

XN-HR; a=7.10617(12) Å, b=4.40625(9) Å, c=6.68269(21) Å

X-IP; a=7.0944(6) Å, b=4.3997(4) Å, c=6.6764(9) Å

XN-IP; a=7.0942(9) Å, b=4.3996(5) Å, c=6.6760(9) Å

* Equivalent isotropic thermal factor

[†] All D atoms are constrained to have the same displacement parameters

[‡] Data used for the refinement; X: SR-XPD data; XN: combined SR-XPD/NPD data

[§] HR: High resolution powder diffractometer; IP: Image plate detector powder diffractometer

B. Influence of the refined structural model on the sharing of the total intensity for overlapping reflections, with and without G-constraints

Large differences in the prior distributions are found between the ones corresponding to a procrystal based on a structural model refined against SR-XPD data or combined SR-XPD/NPD data (See Figs. 1-3 of the main manuscript). This arises from large differences in the refined atomic displacement parameters (ADP) of D atoms between the two types of refinements (see Table II and Table III of the main manuscript). By contrast little differences -one order of magnitude smaller- are found for the ADP of the other atoms and all the refined atomic coordinates. In order to disentangle the double role played by the refined structural model (first: sharing of the total intensity for overlapping reflections; second: prior density distribution) and consider only its role on the sharing of the total intensity for overlapping reflections, almost identical priors distributions have been used for different sets of $F_{obs}(\mathbf{H})$ obtained from refined models against either SR-XPD data or combined SR-XPD/NPD data. The prior densities considered here correspond to a procrystal without considering the thermal smearing of the neutral atoms by the atomic displacements (i.e. prior densities only differ for the atomic coordinates). Hence Fig. 7 and Fig. 8, Fig. 9 and Fig. 10, Fig. 11 and Fig. 12 illustrates for the different temperatures and setups, the MEM densities obtained from two sets of $F_{obs}(\mathbf{H})$ with and without the use of G-constraints. As a general observation, resulting MEM distributions with G-constraints reveal very similar features for two sets of $F_{obs}(\mathbf{H})$ obtained by the two refined models. E.g. for the data at 10 K, for MEM distributions with G-constraint the difference distribution in Fig. 7 exhibit a little positive charge accumulation between the B and D atoms for both sets of $F_{obs}(\mathbf{H})$. For MEM distributions without G-constraints (i.e. forcing -within standard deviations- the calculated MEM structure factors to respect the intensity sharing given by the refined structural model for the overlapping peaks), one can see in the difference distribution in Fig. 8 that for the model refined against SR-XPD data a larger accumulation of charge on the D atoms occurs. The same trend is observed for the MEM distributions corresponding to data at 90 K. Therefore considering group of overlapping peaks as a single reflection reduces the influence of the structural model sufficiently so that similar fine features of the MEM density distributions are exhibited. The refined structural model being -in fine- virtually necessary only for the determination of the scale factor needed to extract the set of $F_{obs}(\mathbf{H})$

and $G_{obs}(\mathbf{H})$ from the experimental data, while guaranteeing appropriate estimates of the standard deviations (e.g. by contrast to a Le Bail fit).

FIG. 7: MEM density distribution for SR-XPD data (high resolution powder diffractometer) at 10 K. Top left (A): Prior density distribution from procrystal refined with combined SR-XPD/NPD data without considering thermal displacement; Top right (B): Prior density distribution from procrystal refined with SR-XPD data without considering thermal displacement; Middle left (C): MEM density distribution using G-constraint from $F_{obs}(\mathbf{H})$ from combined SR-XPD/NPD refined model and prior (A); Middle right (D): MEM density distribution using G-constraint from $F_{obs}(\mathbf{H})$ from combined SR-XPD refined model and prior (B); Bottom left (E): Difference distribution (C-A); Bottom left (F): Difference distribution (D-B). Contour intervals 0.2 e /Å^3, cutoff level 5 e /Å^3. Contour intervals for difference plot 0.1 e /Å^3. Plane cutting D1, D2, and B atoms; Li: green; B: blue; D: red.

FIG. 8: MEM density distribution for SR-XPD data (high resolution powder diffractometer) at 10 K. Top left (A): Prior density distribution from procrystal refined with combined SR-XPD/NPD data without considering thermal displacement; Top right (B): Prior density distribution from procrystal refined with SR-XPD data without considering thermal displacement; Middle left (C): MEM density distribution without G-constraint from $F_{obs}(\mathbf{H})$ from combined SR-XPD/NPD refined model and prior (A); Middle right (D): MEM density distribution without G-constraint from $F_{obs}(\mathbf{H})$ from combined SR-XPD refined model and prior (B); Bottom left (E): Difference distribution (C-A); Bottom left (F): Difference distribution (D-B). Contour intervals 0.2 e /Å^3, cutoff level 5 e /Å^3. Contour intervals for difference plot 0.1 e /Å^3. Plane cutting D1, D2, and B atoms; Li: green; B: blue; D: red.

FIG. 9: MEM density distribution for SR-XPD data (high resolution powder diffractometer) at 90 K. Top left (A): Prior density distribution from procrystal refined with combined SR-XPD/NPD data without considering thermal displacement; Top right (B): Prior density distribution from procrystal refined with SR-XPD data without considering thermal displacement; Middle left (C): MEM density distribution using G-constraint from $F_{obs}(\mathbf{H})$ from combined SR-XPD/NPD refined model and prior (A); Middle right (D): MEM density distribution using G-constraint from $F_{obs}(\mathbf{H})$ from combined SR-XPD refined model and prior (B); Bottom left (E): Difference distribution (C-A); Bottom left (F): Difference distribution (D-B). Contour intervals 0.2 e /Å^3, cutoff level 5 e /Å^3. Contour intervals for difference plot 0.1 e /Å^3. Plane cutting D1, D2, and B atoms; Li: green; B: blue; D: red.

FIG. 10: MEM density distribution for SR-XPD data (high resolution powder diffractometer) at 90 K. Top left (A): Prior density distribution from procrystal refined with combined SR-XPD/NPD data without considering thermal displacement; Top right (B): Prior density distribution from procrystal refined with SR-XPD data without considering thermal displacement; Middle left (C): MEM density distribution without G-constraint from $F_{obs}(\mathbf{H})$ from combined SR-XPD/NPD refined model and prior (A); Middle right (D): MEM density distribution without G-constraint from $F_{obs}(\mathbf{H})$ from combined SR-XPD refined model and prior (B); Bottom left (E): Difference distribution (C-A); Bottom left (F): Difference distribution (D-B). Contour intervals 0.2 e /Å^3, cutoff level 5 e /Å^3. Contour intervals for difference plot 0.1 e /Å^3. Plane cutting D1, D2, and B atoms; Li: green; B: blue; D: red.

FIG. 11: MEM density distribution for SR-XPD data (image plate detector powder diffractometer) at 90 K. Top left (A): Prior density distribution from procrystal refined with combined SR-XPD/NPD data without considering thermal displacement; Top right (B): Prior density distribution from procrystal refined with SR-XPD data without considering thermal displacement; Middle left (C): MEM density distribution using G-constraint from $F_{obs}(\mathbf{H})$ from combined SR-XPD/NPD refined model and prior (A); Middle right (D): MEM density distribution using G-constraint from $F_{obs}(\mathbf{H})$ from combined SR-XPD refined model and prior (B); Bottom left (E): Difference distribution (C-A); Bottom left (F): Difference distribution (D-B). Contour intervals 0.2 e /Å^3, cutoff level 5 e /Å^3. Contour intervals for difference plot 0.1 e /Å^3. Plane cutting D1, D2, and B atoms; Li: green; B: blue; D: red.

FIG. 12: MEM density distribution for SR-XPD data (image plate detector powder diffractometer) at 90 K. Top left (A): Prior density distribution from procrystal refined with combined SR-XPD/NPD data without considering thermal displacement; Top right (B): Prior density distribution from procrystal refined with SR-XPD data without considering thermal displacement; Middle left (C): MEM density distribution without G-constraint from $F_{obs}(\mathbf{H})$ from combined SR-XPD/NPD refined model and prior (A); Middle right (D): MEM density distribution without G-constraint from $F_{obs}(\mathbf{H})$ from combined SR-XPD refined model and prior (B); Bottom left (E): Difference distribution (C-A); Bottom left (F): Difference distribution (D-B). Contour intervals 0.2 e /Å^3, cutoff level 5 e /Å^3. Contour intervals for difference plot 0.1 e /Å^3. Plane cutting D1, D2, and B atoms; Li: green; B: blue; D: red.

C. Influence of prior density distribution considering different structural models for a given set of $F_{obs}(\mathbf{H})$

Since G-constraints reduces the influence of the refined structural model to a sufficient level to distinguish similar features (see above discussion), the differences between MEM distributions obtained for the same set of $F_{obs}(\mathbf{H})$ and different priors may essentially result from a direct influence of the prior density. This is qualitatively illustrated in Fig. 13, and clearly the prior density distribution stands out as one of the initial assumptions influencing the most the resulting MEM distributions, i.e. through which the choice of the refined structural model influences the most the resulting MEM distributions. Actually, it is a direct consequence of the accuracy of the $F_{obs}(\mathbf{H})$, hence indirectly, of the collected data. The reason is that at the end of a MEM calculations, the structure factors corresponding to the calculated distribution $F_{MEM}(\mathbf{H})$ are as close to the experimental $F_{obs}(\mathbf{H})$ as allowed by the standard deviation $\sigma_{obs}(\mathbf{H})$ via the χ^2 constraint. In an extreme case, for inaccurate data yielding very large $\sigma_{obs}(\mathbf{H})$, the constraint χ^2 might be almost already satisfied for the prior distribution τ, thus $\rho \approx \tau$. By contrast, accurate data yielding small $\sigma_{obs}(\mathbf{H})$ forces the $F_{MEM}(\mathbf{H})$ of the final distribution ρ to be closer to the $F_{obs}(\mathbf{H})$ to satisfy the constraint χ^2, hence reducing the influence of the initial distribution τ on the final distribution ρ.

FIG. 13: MEM density distribution for SR-XPD data at 10 K. Top left (A): Prior density distribution from procrystal refined with combined SR-XPD/NPD data ; Top right (B): Prior density distribution from procrystal refined with SR-XPD data; Middle left (C): MEM density distribution with G-constraint from $F_{obs}(\mathbf{H})$ from combined SR-XPD/NPD refined model and prior (A); Middle right (D): MEM density distribution with G-constraint from $F_{obs}(\mathbf{H})$ from combined SR-XPD refined model and prior (B); Bottom left (E): MEM density distribution with G-constraint from $F_{obs}(\mathbf{H})$ from combined SR-XPD/NPD refined model and prior (B); Middle right (E): MEM density distribution with G-constraint from $F_{obs}(\mathbf{H})$ from SR-XPD refined model and prior (A). Contour intervals 0.2 e /Å^3, cutoff level 5 e /Å^3. Plane cutting D1, D2, and B atoms; Li: green; B: blue; D: red.

D. Influence of the order of the statistical central moment of the normal residuals of the structure factors

The consideration of higher-order central moments for the distribution of the residuals of the structure factors $\left(|F_{obs}(\mathbf{H})| - |F_{MEM}(\mathbf{H})|\right)/\sigma(\mathbf{H})$ did not result in a significant change of the resulting MEM distributions (see Fig. 14, Fig. 15, and Fig. 16) and the classical order 2 (i.e. χ^2) constraint has been considered for the convergence criterion of MEM calculations. This is further reflected in Tables II and III of the main manuscript, where differences of atomic charges obtained for different orders are smaller than the accuracy of these atomic charges.

FIG. 14: MEM density distribution for data at 10 K, with G constraints, and from $F_{obs}(\mathbf{H})$ from combined SR-XPD/NPD refined model and prior. Top left: statistical moment χ^2; Top right: statistical moment χ^4; Bottom: statistical moment χ^6. Contour intervals 0.2 e /Å^3, cutoff level 5 e /Å^3. Plane cutting D1, D2, and B atoms; Li: green; B: blue; D: red.

FIG. 15: MEM density distribution for data at 90 K (high resolution powder diffractometer), with G constraints, and from $F_{obs}(\mathbf{H})$ from combined SR-XPD/NPD refined model and prior. Top left: statistical moment χ^2; Top right: statistical moment χ^4; Bottom: statistical moment χ^6. Contour intervals 0.2 e /Å^3, cutoff level 5 e /Å^3. Plane cutting D1, D2, and B atoms; Li: green; B: blue; D: red.

FIG. 16: MEM density distribution for data at 90 K (image plate detector powder diffractometer), with G constraints, and from $F_{obs}(\mathbf{H})$ from combined SR-XPD/NPD refined model and prior. Top left: statistical moment χ^2; Top right: statistical moment χ^4; Bottom: statistical moment χ^6. Contour intervals 0.2 e /Å^3, cutoff level 5 e /Å^3. Plane cutting D1, D2, and B atoms; Li: green; B: blue; D: red.

E. Influence of the use of prior-derived F constraints

Introducing prior-derived F constraints for the non-measured structure factors up to a chosen high scattering angle limit (i.e. for $0.6\ \text{Å}^{-1} \leq \sin\theta/\lambda \leq 2.5\ \text{Å}^{-1}$ in the present case) was considered to possibly reduce artifacts in the MEM density distributions. In absolute value, the introduction of these constraints changes the MEM density distributions somewhat more than the effect of different higher-order central moments for the distribution of the residuals of the structure factors (see Fig 17, Fig 18, and Fig 19). However, the density distribution (curvature) at the border between the atomic basins (determining the zero-flux surfaces, hence the atomic charges) corresponding to B and D depends a lot on the prior distribution. For a prior refined against combined SR-XPD/NPD data, the use of prior-derived F constraints does not change the final MEM distribution significantly. By contrast, a prior refined against SR-XPD data, the use of prior-derived F constraints does change a lot the curvature of the final MEM distribution between the atomic basins (see Fig 17, Fig 18 and the corresponding atomic charges (see Tables II and III of the main manuscript). Compared to the MEM distribution without prior-derived F constraints (see Fig 17, Fig 18), the minimum of density (roughly indicating the zero-flux surfaces and bond critical points[?]) are shifted towards B. Therefore, due to the approximations in the refined structural model used to determine the prior-derived F constraints (due to the B-D covalent bond and the non existence of core electrons in D), and the maximal measured scattering angle which stands below the limit $\sin\theta/\lambda \geq 0.9\ \text{Å}^{-1}$ for which higher scattering angle are assumed to correspond to core electrons, no prior-derived F constraints have been considered for the final MEM distributions.

FIG. 17: MEM density distribution for data at 10 K, with G constraints. Top: without prior F-constraint; Bottom: with prior F-constraint ($\leq 0.6\mathring{A}\frac{\sin\theta}{\lambda} \leq 2.5\mathring{A}$); Left: from $F_{obs}(\mathbf{H})$ from combined SR-XPD/NPD refined model and prior; right: from $F_{obs}(\mathbf{H})$ from SR-XPD refined model and prior. Contour intervals 0.2 e /Å^3, cutoff level 5 e /Å^3. Plane cutting D1, D2, and B atoms; Li: green; B: blue; D: red.

FIG. 18: MEM density distribution for data at 90 K (high resolution powder diffractometer), with G constraints. Top: without prior F-constraint; Bottom: with prior F-constraint ($\leq 0.6\mathring{A}\frac{\sin\theta}{\lambda} \leq 2.5\mathring{A}$); Left: from $F_{obs}(\mathbf{H})$ from combined SR-XPD/NPD refined model and prior; right: from $F_{obs}(\mathbf{H})$ from SR-XPD refined model and prior. Contour intervals 0.2 e /Å^3, cutoff level 5 e /Å^3. Plane cutting D1, D2, and B atoms; Li: green; B: blue; D: red.

FIG. 19: MEM density distribution for data at 90 K (image plate detector powder diffractometer), with G constraints. Top: without prior F-constraint; Bottom: with prior F-constraint ($\leq 0.6\mathring{A}\frac{\sin\theta}{\lambda} \leq 2.5\mathring{A}$); Left: from $F_{obs}(\mathbf{H})$ from combined SR-XPD/NPD refined model and prior; right: from $F_{obs}(\mathbf{H})$ from SR-XPD refined model and prior. Contour intervals 0.2 e /Å^3, cutoff level 5 e /Å^3. Plane cutting D1, D2, and B atoms; Li: green; B: blue; D: red.

F. Influence of covalent bond on refined atomic positions

FIG. 20: Prior density distribution from a procrystal corresponding to a model refined against SR-XPD data, and without considering thermal displacements. Atomic positions correspond to a model refined against combined SR-XPD/NPD data; Along the B-D path, there is a shift towards the B atom of the maximal density corresponding to the model refined against SR-XPD data with respect to the atomic positions refined against combined SR-XPD/NPD data. Top left: 10 K; Top right: 90 K (high resolution powder diffractometer); Bottom: (image plate detector powder diffractometer). Contour intervals 0.2 e /Å^3, cutoff level 5 e /Å^3. Plane cutting D1, D2, and B atoms; Li: green; B: blue; D: red.

---

[*] Also at University of Fribourg, Physics Department, CH-1700 Fribourg, Switzerland; Electronic address: `florian.buchter@empa.ch`

[†] Also at University of Fribourg, Physics Department, CH-1700 Fribourg, Switzerland

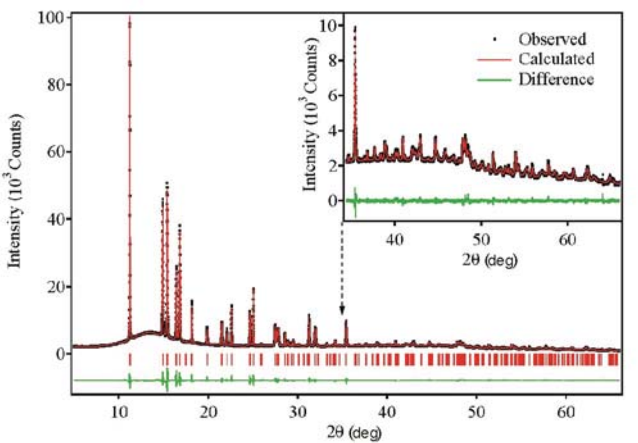
Observed
Calculated
Difference
Intensity (10^3 Counts)
2θ (deg)
100
80
60
40
20
0
10
20
30
40
50
60
10
8
6
4
2
0

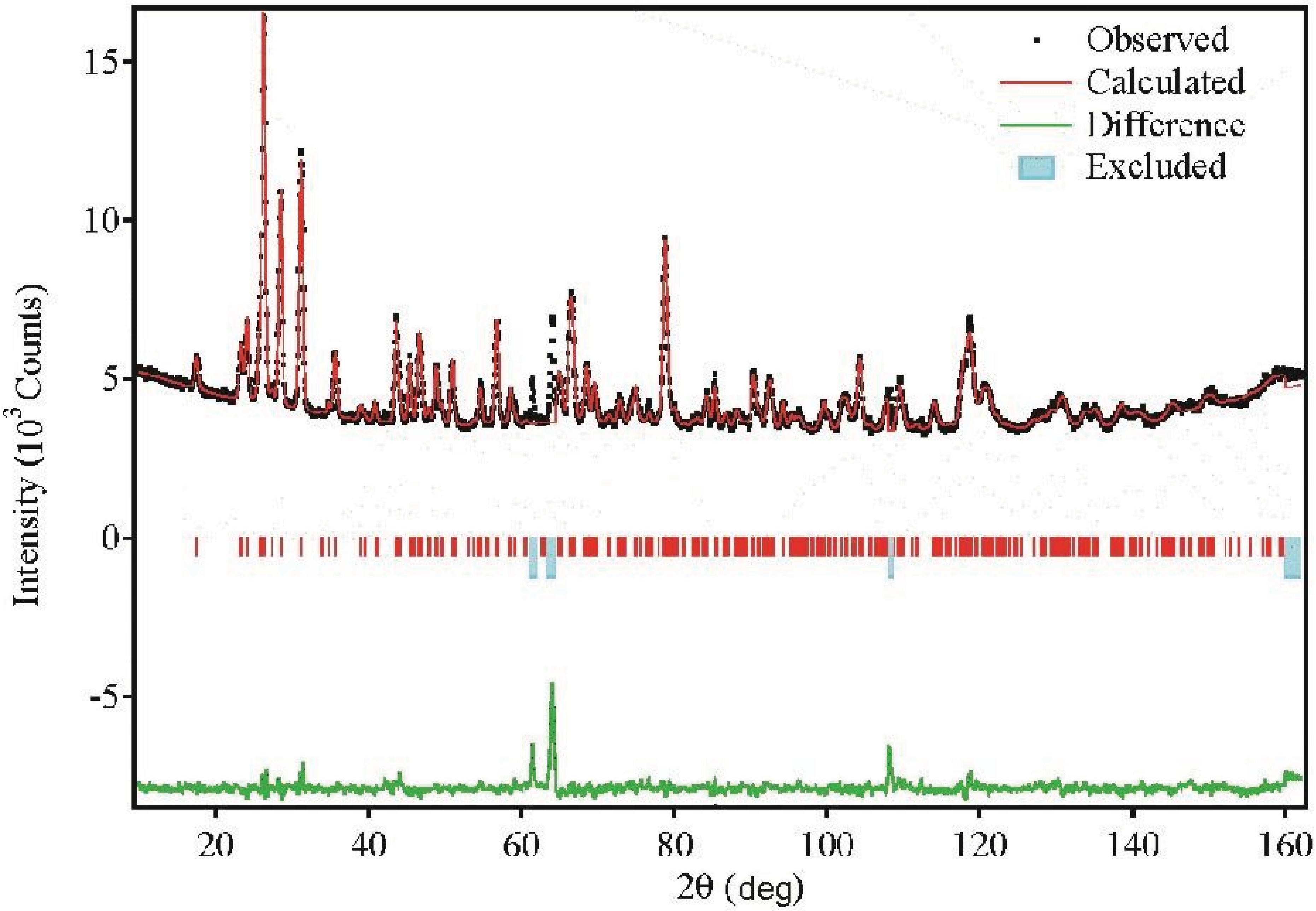
Observed
Calculated
Difference
Excluded
Intensity (10^3 Counts)
15
10
5
0
-5
20
40
60
80
100
120
140
160
2θ (deg)

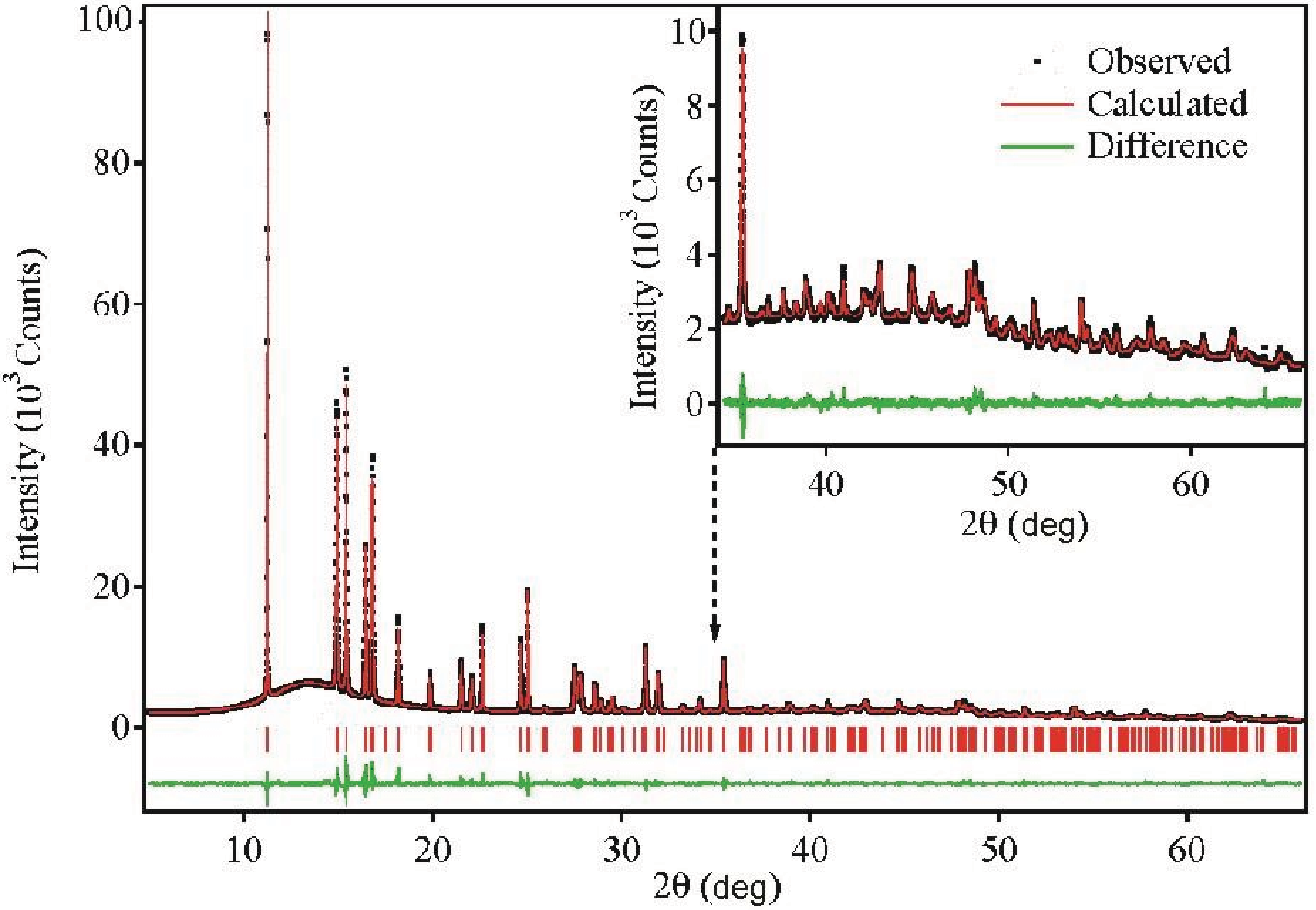
Observed
Calculated
Difference
Intensity (10^3 Counts)
100
80
60
40
20
0
10
20
30
40
50
60
2θ (deg)
Intensity (10^3 Counts)
10
8
6
4
2
0
40
50
60
2θ (deg)

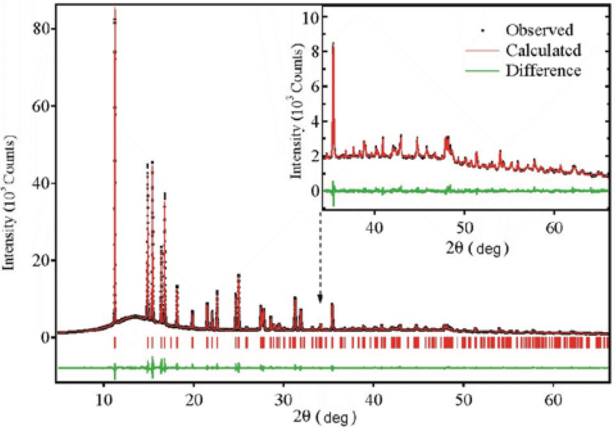
Observed
Calculated
Difference
Intensity (10^3 Counts)
2θ (deg)
0
20
40
60
80
10
20
30
40
50
60
0
2
4
6
8
10
40
50
60

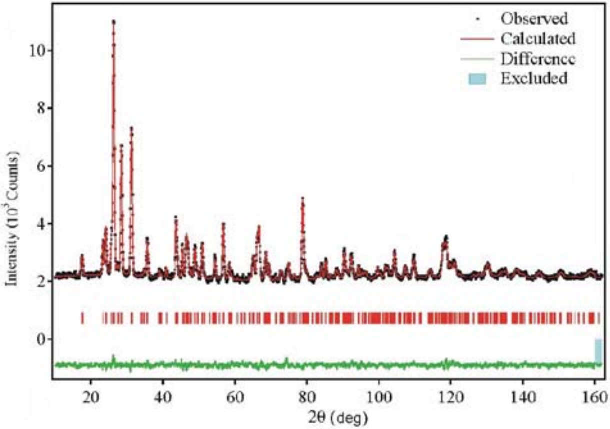
Observed
Calculated
Difference
Excluded
Intensity (10^3 Counts)
0
2
4
6
8
10
20
40
60
80
100
120
140
160
2θ (deg)

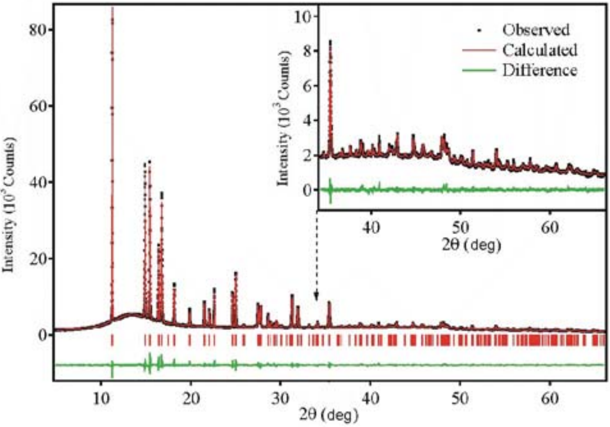
Observed
Calculated
Difference
Intensity (10^3 Counts)
0
2
4
6
8
10
40
50
60
2θ (deg)
Intensity (10^3 Counts)
0
20
40
60
80
10
20
30
40
50
60
2θ (deg)

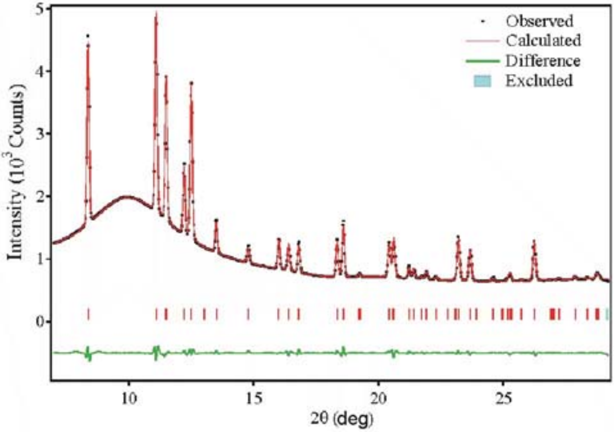
Observed
Calculated
Difference
Excluded
Intensity (10^3 Counts)
5
4
3
2
1
0
10
15
20
25
2θ (deg)

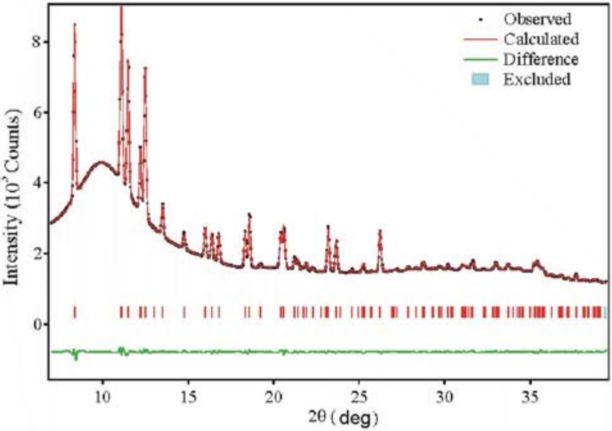
Observed
Calculated
Difference
Excluded
Intensity (10^3 Counts)
8
6
4
2
0
10
15
20
25
30
35
2θ (deg)

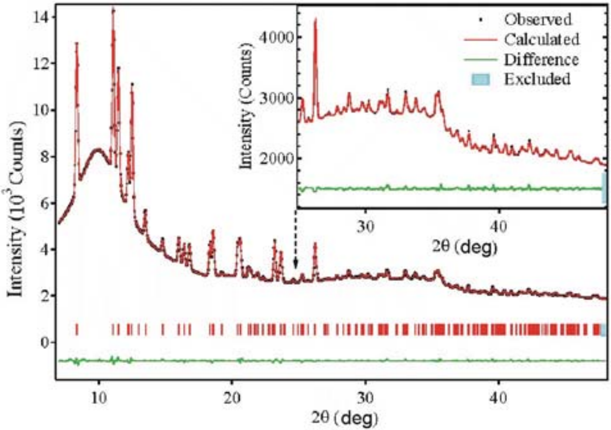
Observed
Calculated
Difference
Excluded
Intensity (Counts)
4000
3000
2000
30
40
2θ (deg)
Intensity (10^3 Counts)
14
12
10
8
6
4
2
0
10
20
30
40
2θ (deg)

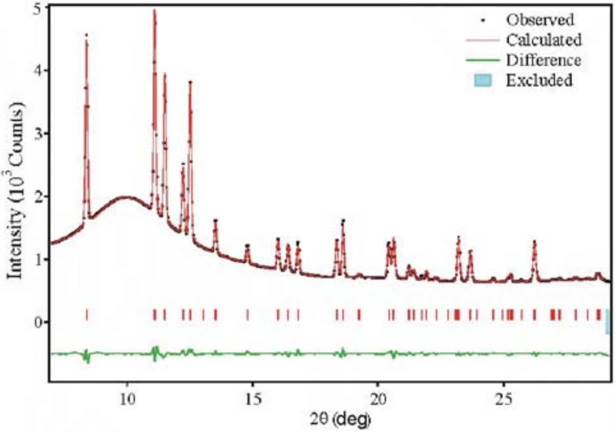
Observed
Calculated
Difference
Excluded
Intensity (10^3 Counts)
0
1
2
3
4
5
10
15
20
25
2θ (deg)

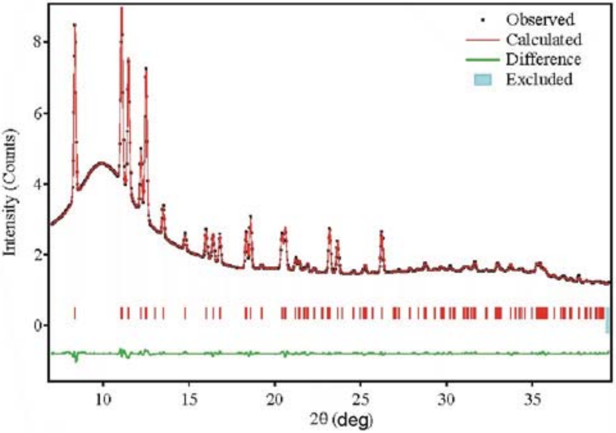
Observed
Calculated
Difference
Excluded
Intensity (Counts)
0
2
4
6
8
10
15
20
25
30
35
2θ (deg)

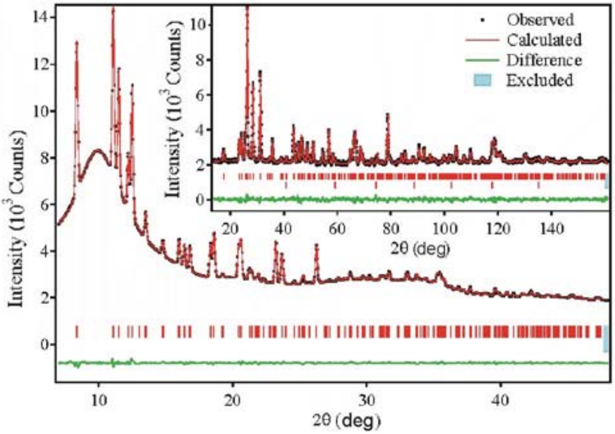
Observed
Calculated
Difference
Excluded
Intensity (10^3 Counts)
0
2
4
6
8
10
20
40
60
80
100
120
140
2θ (deg)
Intensity (10^3 Counts)
0
2
4
6
8
10
12
14
10
20
30
40
2θ (deg)

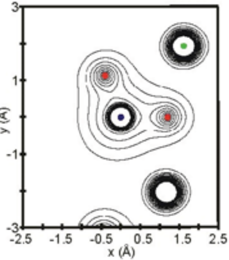
3
1
-1
-3
y (Å)
-2.5 -1.5 -0.5 0.5 1.5 2.5
x (Å)

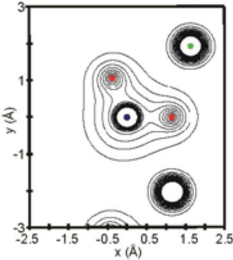
3
1
-1
-3
y (Å)
-2.5 -1.5 -0.5 0.5 1.5 2.5
x (Å)

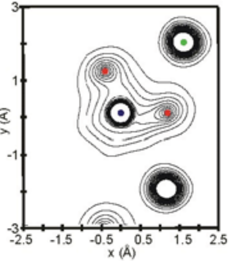
3
1
-1
-3
y (Å)
-2.5 -1.5 -0.5 0.5 1.5 2.5
x (Å)

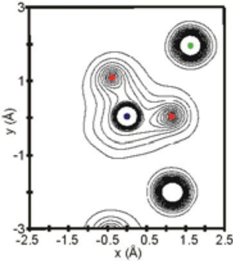
3
1
-1
-3
y (Å)
-2.5 -1.5 -0.5 0.5 1.5 2.5
x (Å)

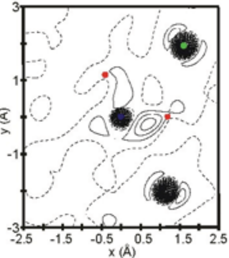
3
1
-1
-3
y (Å)
-2.5 -1.5 -0.5 0.5 1.5 2.5
x (Å)

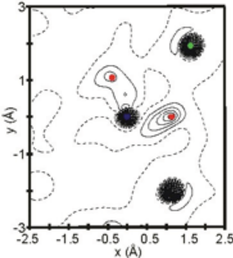
3
1
-1
-3
y (Å)
-2.5 -1.5 -0.5 0.5 1.5 2.5
x (Å)

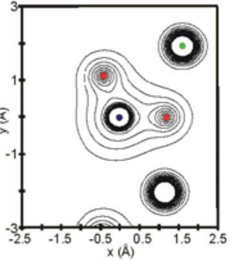
3
1
-1
-3
y (Å)
-2.5 -1.5 -0.5 0.5 1.5 2.5
x (Å)

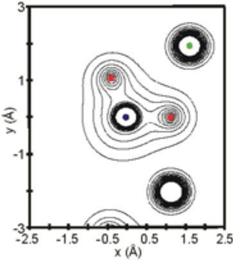
3
1
-1
-3
y (Å)
-2.5 -1.5 -0.5 0.5 1.5 2.5
x (Å)

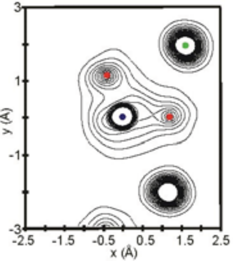
3
1
-1
-3
y (Å)
-2.5 -1.5 -0.5 0.5 1.5 2.5
x (Å)

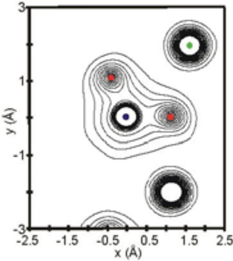
3
1
-1
-3
y (Å)
-2.5 -1.5 -0.5 0.5 1.5 2.5
x (Å)

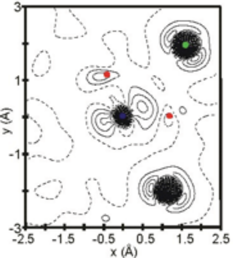
3
1
-1
-3
y (Å)
-2.5 -1.5 -0.5 0.5 1.5 2.5
x (Å)

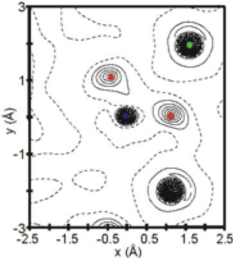
3
1
-1
-3
y (Å)
-2.5 -1.5 -0.5 0.5 1.5 2.5
x (Å)

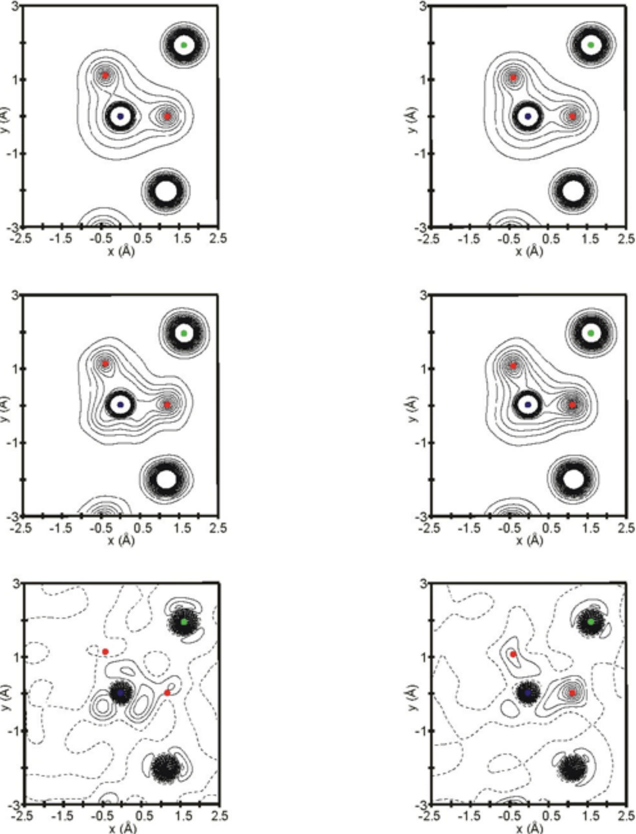
3
1
-1
-3
y (Å)
-2.5
-1.5
-0.5
0.5
1.5
2.5
x (Å)

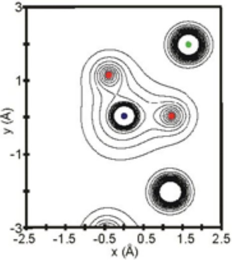
3
1
-1
-3
y (Å)
-2.5
-1.5
-0.5
0.5
1.5
2.5
x (Å)

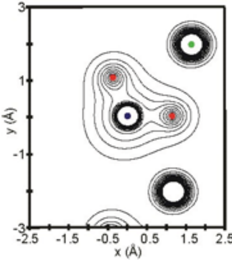
3
1
-1
-3
y (Å)
-2.5
-1.5
-0.5
0.5
1.5
x (Å)

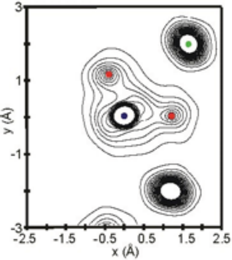
3
1
-1
-3
y (Å)
-2.5
-1.5
-0.5
0.5
1.5
2.5
x (Å)

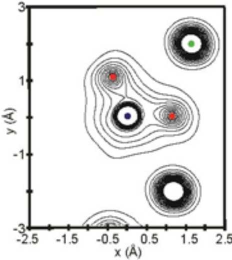
3
1
-1
-3
y (Å)
-2.5
-1.5
-0.5
0.5
1.5
x (Å)

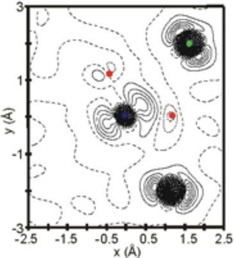
3
1
-1
-3
y (Å)
-2.5
-1.5
-0.5
0.5
1.5
2.5
x (Å)

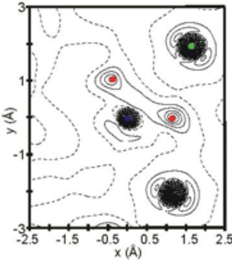
3
1
-1
-3
y (Å)
-2.5
-1.5
-0.5
0.5
1.5
x (Å)

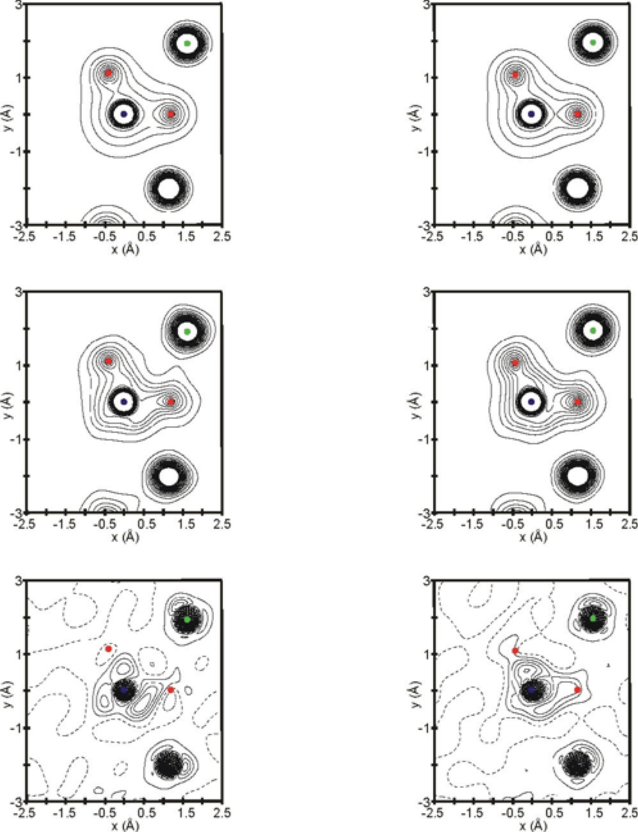

3
1
-1
-3
y (Å)
-2.5
-1.5
-0.5
0.5
1.5
2.5
x (Å)
3
1
-1
-3
y (Å)
-2.5
-1.5
-0.5
0.5
1.5
2.5
x (Å)
3
1
-1
-3
y (Å)
-2.5
-1.5
-0.5
0.5
1.5
2.5
x (Å)
3
1
-1
-3
y (Å)
-2.5
-1.5
-0.5
0.5
1.5
2.5
x (Å)
3
1
-1
-3
y (Å)
-2.5
-1.5
-0.5
0.5
1.5
2.5
x (Å)
3
1
-1
-3
y (Å)
-2.5
-1.5
-0.5
0.5
1.5
2.5
x (Å)

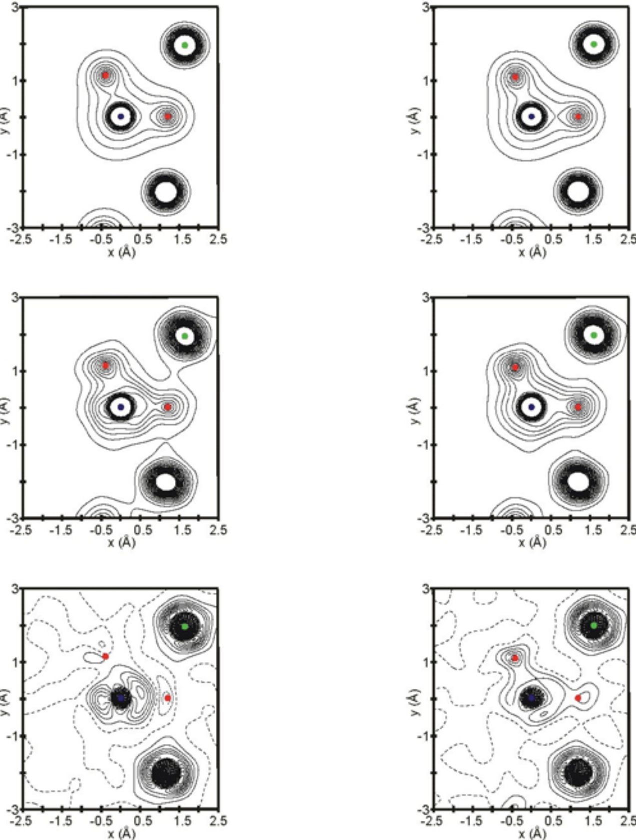

3
1
-1
-3
y (Å)
-2.5
-1.5
-0.5
0.5
1.5
2.5
x (Å)

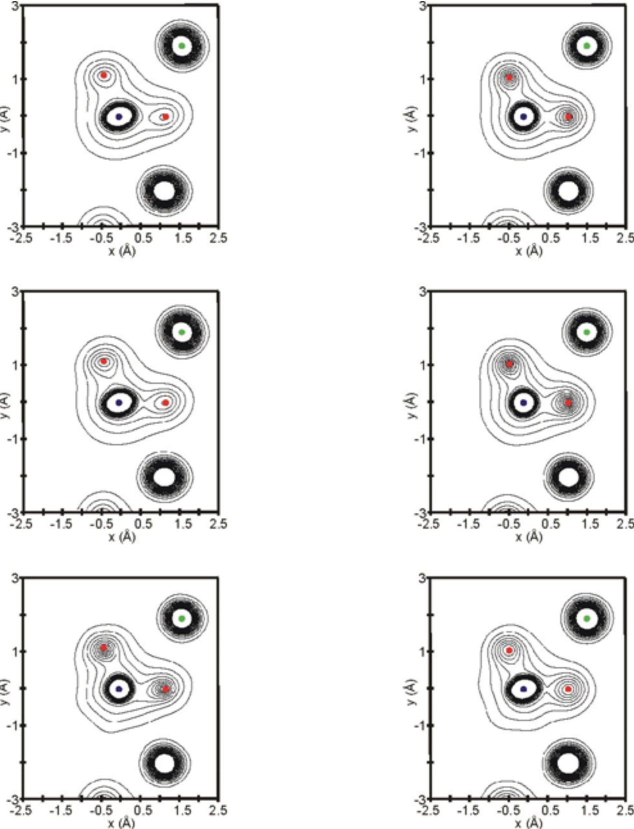
3
1
y (Å)
-1
-3
-2.5
-1.5
-0.5
0.5
1.5
2.5
x (Å)

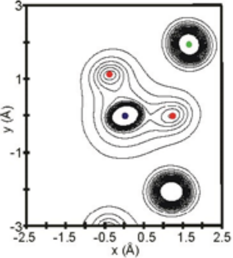
3
1
-1
-3
y (Å)
-2.5
-1.5
-0.5
0.5
1.5
2.5
x (Å)

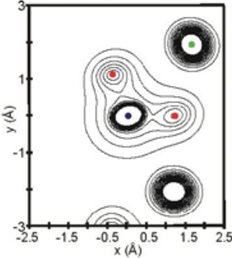
3
1
-1
-3
y (Å)
-2.5
-1.5
-0.5
0.5
1.5
2.5
x (Å)

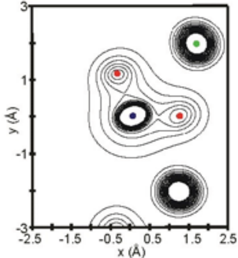
3
1
-1
-3
y (Å)
-2.5
-1.5
-0.5
0.5
1.5
2.5
x (Å)

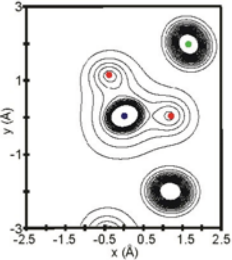
3
1
y (Å)
-1
-3
-2.5
-1.5
-0.5
0.5
1.5
2.5
x (Å)

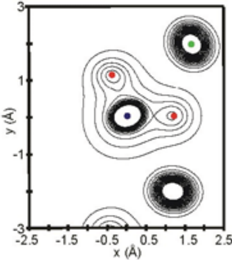
3
1
y (Å)
-1
-3
-2.5
-1.5
-0.5
0.5
1.5
2.5
x (Å)

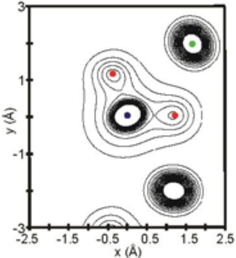
3
1
y (Å)
-1
-3
-2.5
-1.5
-0.5
0.5
1.5
2.5
x (Å)

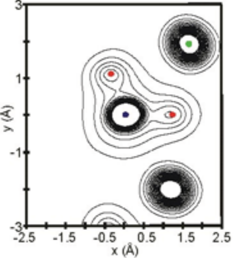
3
1
-1
-3
y (Å)
-2.5
-1.5
-0.5
0.5
1.5
2.5
x (Å)

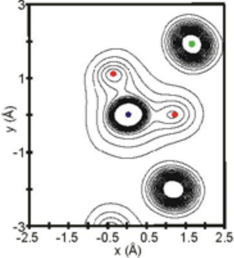
3
1
-1
-3
y (Å)
-2.5
-1.5
-0.5
0.5
1.5
2.5
x (Å)

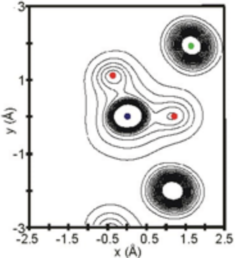
3
1
-1
-3
y (Å)
-2.5
-1.5
-0.5
0.5
1.5
2.5
x (Å)

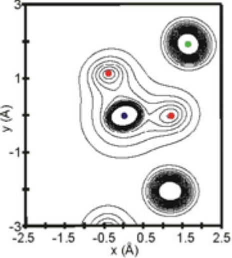

3
1
-1
-3
y (Å)
-2.5
-1.5
-0.5
0.5
1.5
2.5
x (Å)

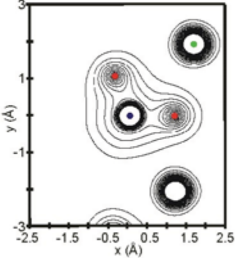

3
1
-1
-3
y (Å)
-2.5
-1.5
-0.5
0.5
1.5
2.5
x (Å)

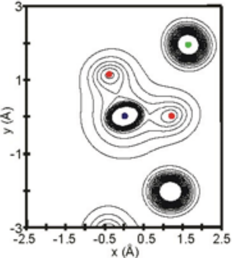

3
1
-1
-3
y (Å)
-2.5
-1.5
-0.5
0.5
1.5
2.5
x (Å)

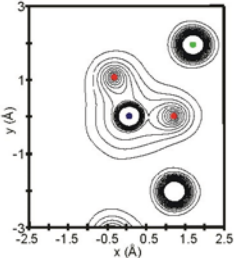

3
1
-1
-3
y (Å)
-2.5
-1.5
-0.5
0.5
1.5
2.5
x (Å)

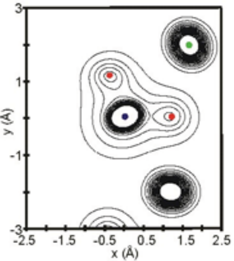
3
1
-1
-3
y (Å)
-2.5
-1.5
-0.5
0.5
1.5
2.5
x (Å)

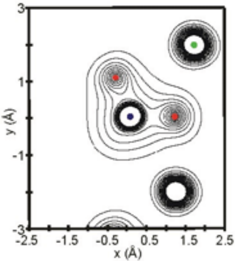
3
1
-1
-3
y (Å)
-2.5
-1.5
-0.5
0.5
1.5
2.5
x (Å)

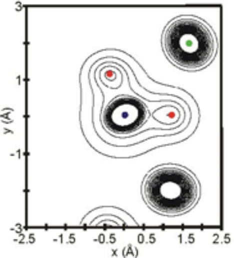
3
1
-1
-3
y (Å)
-2.5
-1.5
-0.5
0.5
1.5
2.5
x (Å)

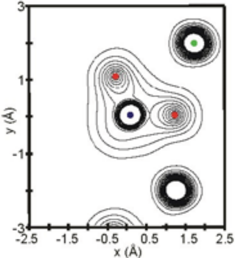
3
1
-1
-3
y (Å)
-2.5
-1.5
-0.5
0.5
1.5
2.5
x (Å)

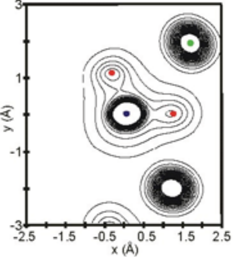
3
1
-1
-3
y (Å)
-2.5
-1.5
-0.5
0.5
1.5
2.5
x (Å)

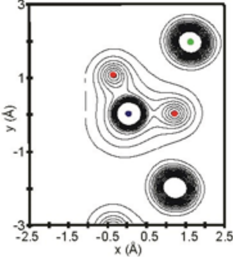
3
1
-1
-3
y (Å)
-2.5
-1.5
-0.5
0.5
1.5
2.5
x (Å)

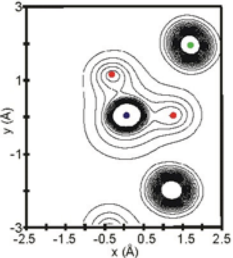
3
1
-1
-3
y (Å)
-2.5
-1.5
-0.5
0.5
1.5
2.5
x (Å)

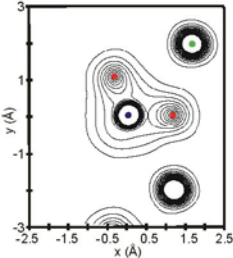
3
1
-1
-3
y (Å)
-2.5
-1.5
-0.5
0.5
1.5
2.5
x (Å)

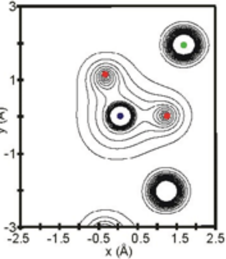
3
1
-1
-3
y (Å)
-2.5
-1.5
-0.5
0.5
1.5
2.5
x (Å)

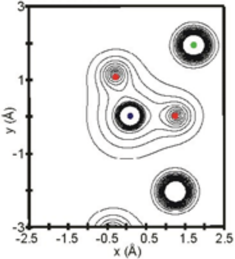
3
1
-1
-3
y (Å)
-2.5
-1.5
-0.5
0.5
1.5
2.5
x (Å)

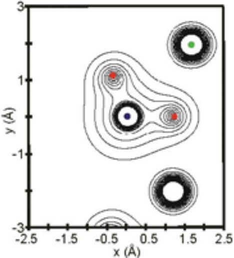
3
1
-1
-3
y (Å)
-2.5
-1.5
-0.5
0.5
1.5
2.5
x (Å)

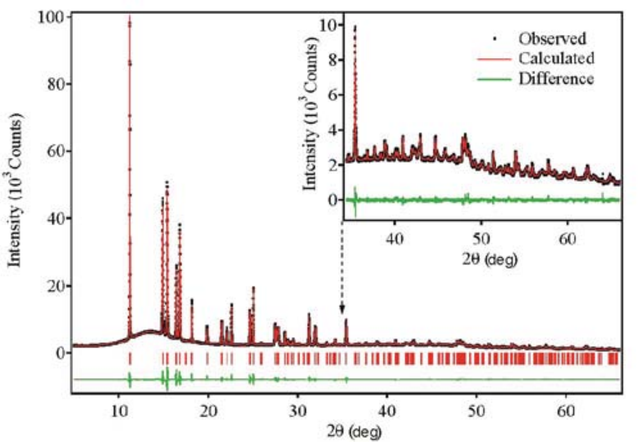

Intensity (10^3 Counts)
100
80
60
40
20
0
10
20
30
40
50
60
2θ (deg)
Observed
Calculated
Difference
Intensity (10^3 Counts)
10
8
6
4
2
0
40
50
60
2θ (deg)

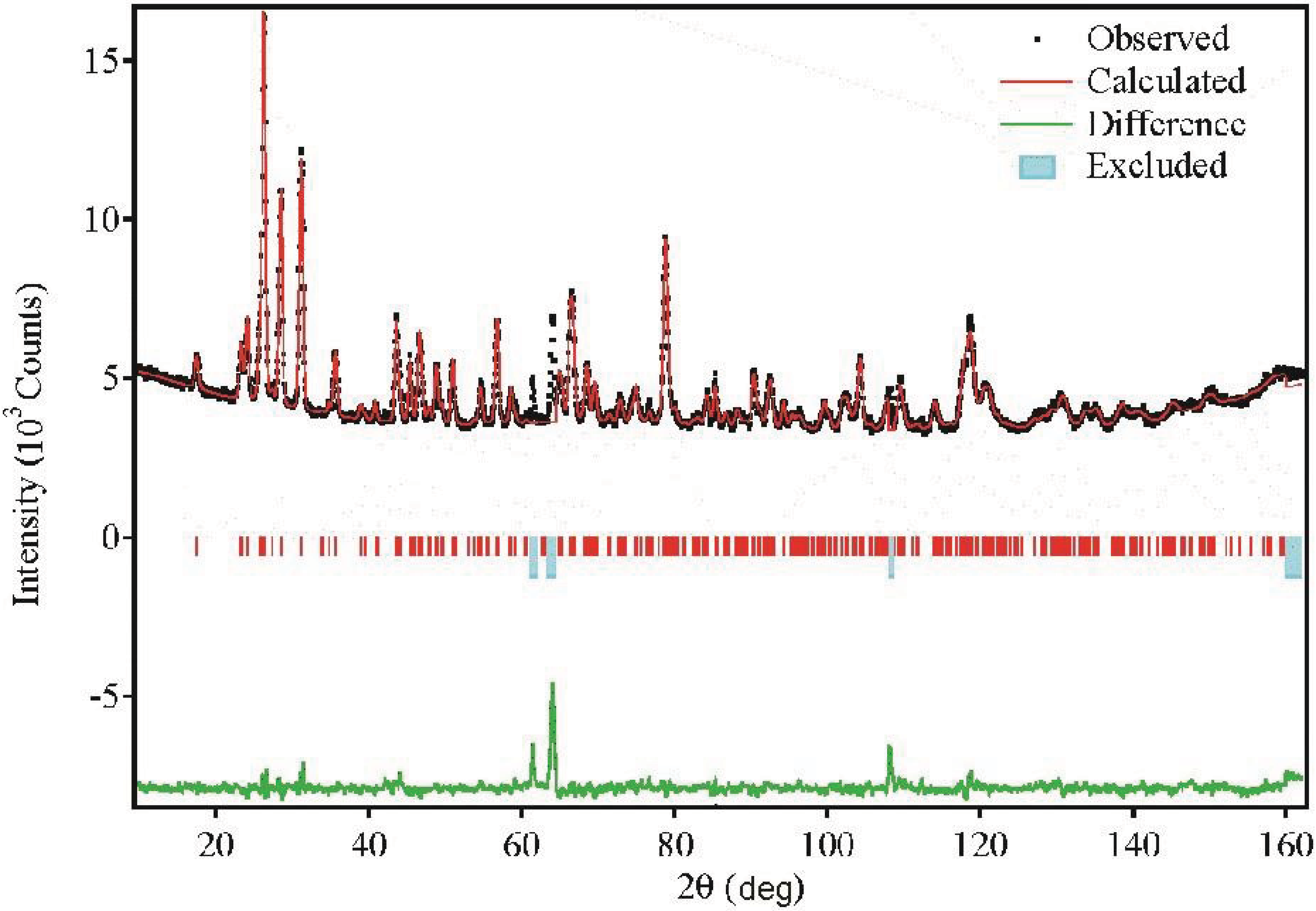
Observed
Calculated
Difference
Excluded
Intensity (10^3 Counts)
15
10
5
0
-5
20
40
60
80
100
120
140
160
2θ (deg)

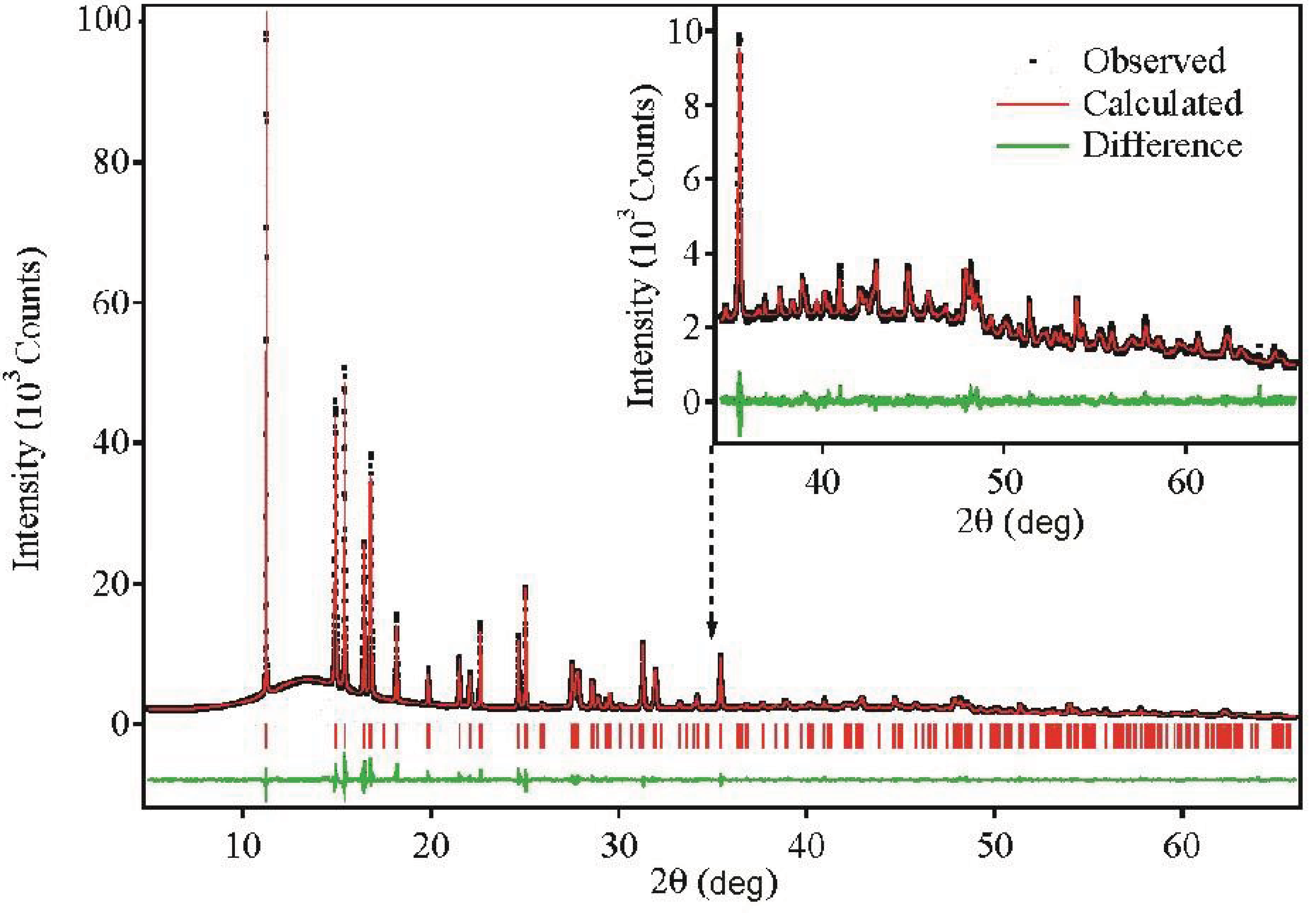
Observed
Calculated
Difference
Intensity (10^3 Counts)
100
80
60
40
20
0
10
20
30
40
50
60
2θ (deg)
Intensity (10^3 Counts)
10
8
6
4
2
0
40
50
60
2θ (deg)

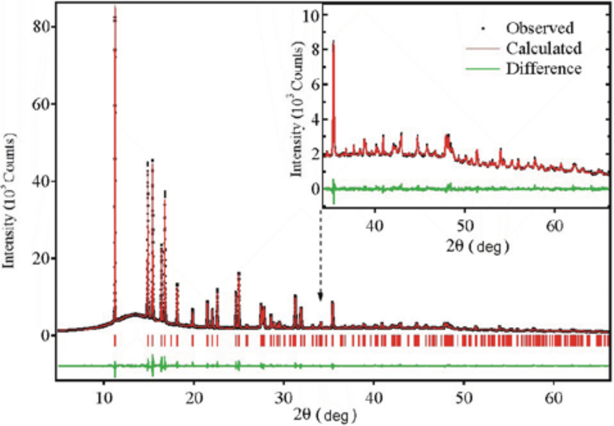
Observed
Calculated
Difference
Intensity (10^3 Counts)
0
2
4
6
8
10
40
50
60
2θ (deg)
Intensity (10^3 Counts)
0
20
40
60
80
10
20
30
40
50
60
2θ (deg)

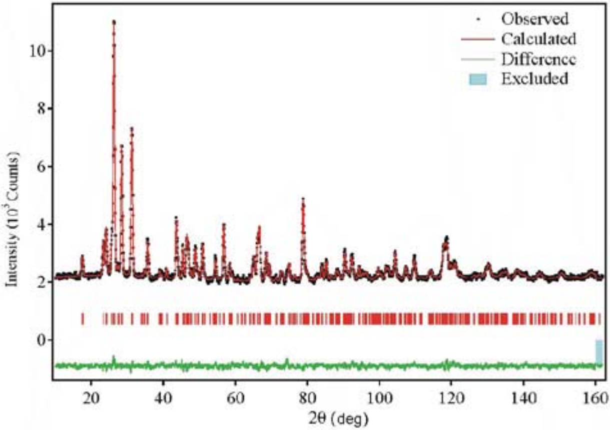

Observed
Calculated
Difference
Excluded
Intensity (10^3 Counts)
2θ (deg)
0
2
4
6
8
10
20
40
60
80
100
120
140
160

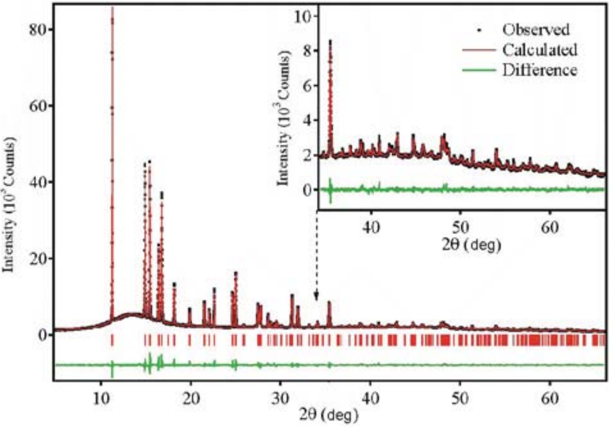

Observed
Calculated
Difference
Intensity (10^3 Counts)
2θ (deg)
0
20
40
60
80
10
20
30
40
50
60
0
2
4
6
8
10
40
50
60

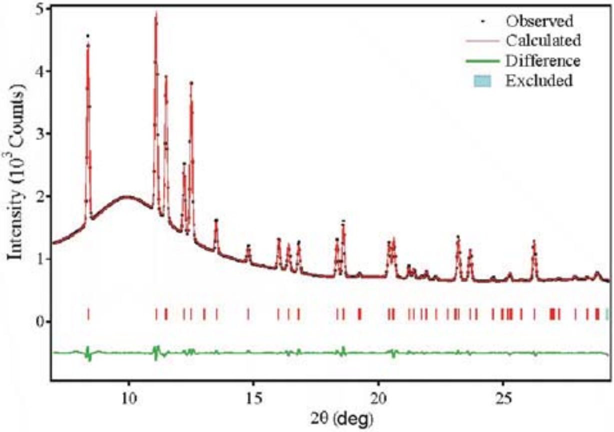
Observed
Calculated
Difference
Excluded
Intensity (10^3 Counts)
0
1
2
3
4
5
10
15
20
25
2θ (deg)

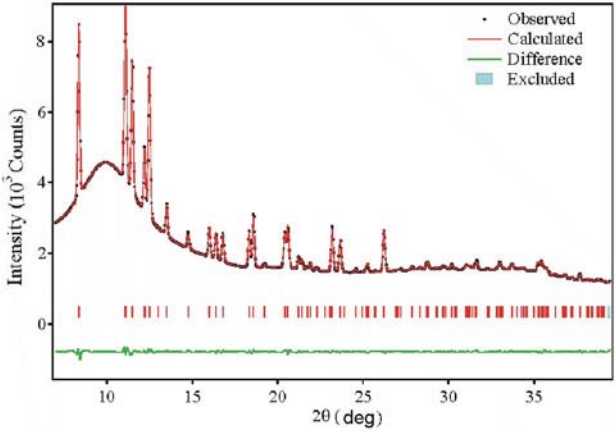
Observed
Calculated
Difference
Excluded
Intensity (10^3 Counts)
0
2
4
6
8
10
15
20
25
30
35
2θ (deg)

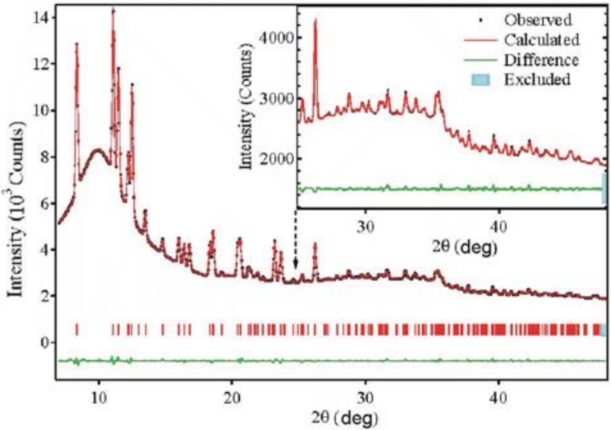
Observed
Calculated
Difference
Excluded
Intensity (Counts)
2000
3000
4000
30
40
2θ (deg)
Intensity (10^3 Counts)
0
2
4
6
8
10
12
14
10
20
30
40
2θ (deg)

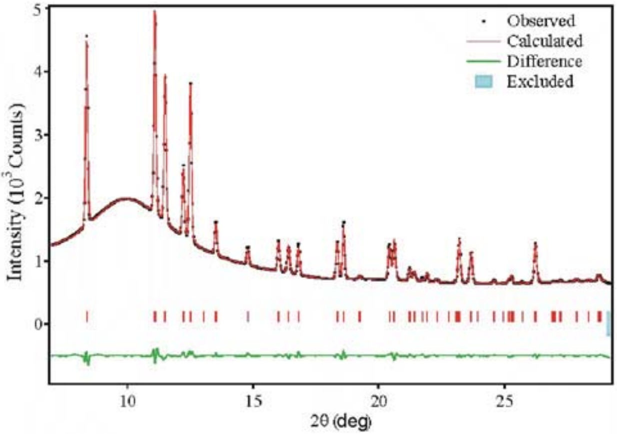
Observed
Calculated
Difference
Excluded
Intensity (10^3 Counts)
0
1
2
3
4
5
10
15
20
25
2θ (deg)

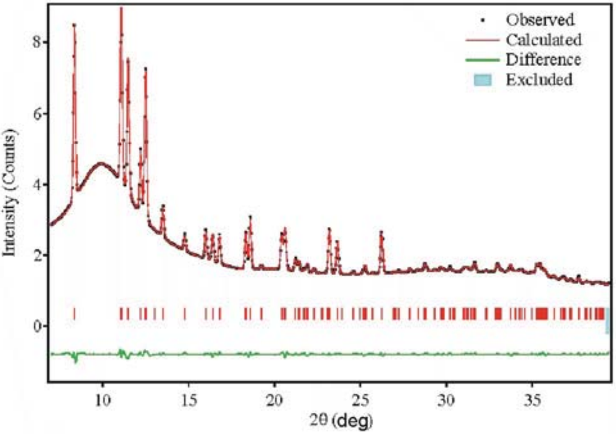
Observed
Calculated
Difference
Excluded
Intensity (Counts)
0
2
4
6
8
10
15
20
25
30
35
2θ (deg)

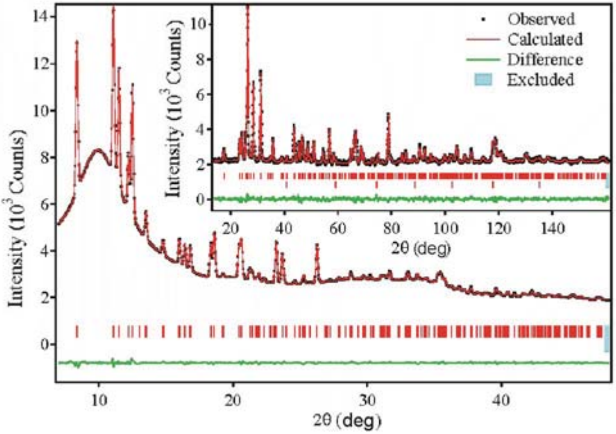
Observed
Calculated
Difference
Excluded
Intensity (10^3 Counts)
0
2
4
6
8
10
20
40
60
80
100
120
140
2θ (deg)
Intensity (10^3 Counts)
0
2
4
6
8
10
12
14
10
20
30
40
2θ (deg)

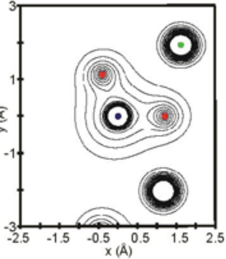
3
1
-1
-3
y (Å)
-2.5
-1.5
-0.5
0.5
1.5
2.5
x (Å)

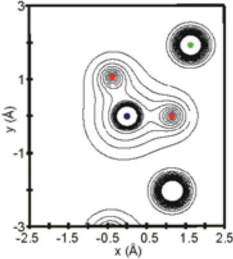
3
1
-1
-3
y (Å)
-2.5
-1.5
-0.5
0.5
1.5
2.5
x (Å)

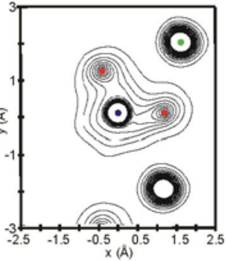
3
1
-1
-3
y (Å)
-2.5
-1.5
-0.5
0.5
1.5
2.5
x (Å)

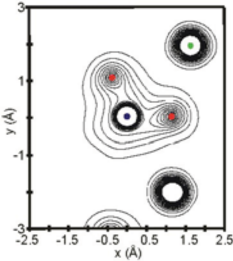
3
1
-1
-3
y (Å)
-2.5
-1.5
-0.5
0.5
1.5
2.5
x (Å)

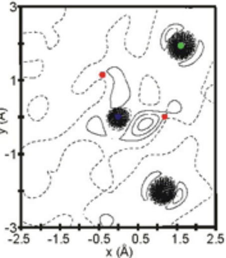
3
1
-1
-3
y (Å)
-2.5
-1.5
-0.5
0.5
1.5
2.5
x (Å)

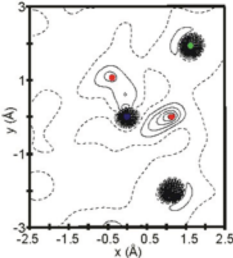
3
1
-1
-3
y (Å)
-2.5
-1.5
-0.5
0.5
1.5
2.5
x (Å)

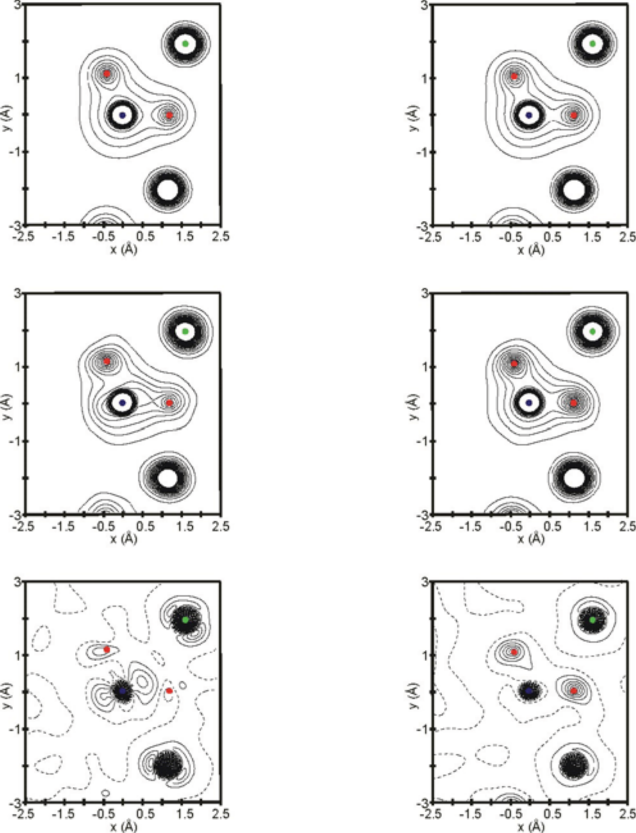
3
1
-1
-3
y (Å)
-2.5
-1.5
-0.5
0.5
1.5
2.5
x (Å)
3
1
-1
-3
y (Å)
-2.5
-1.5
-0.5
0.5
1.5
2.5
x (Å)
3
1
-1
-3
y (Å)
-2.5
-1.5
-0.5
0.5
1.5
2.5
x (Å)
3
1
-1
-3
y (Å)
-2.5
-1.5
-0.5
0.5
1.5
2.5
x (Å)
3
1
-1
-3
y (Å)
-2.5
-1.5
-0.5
0.5
1.5
2.5
x (Å)
3
1
-1
-3
y (Å)
-2.5
-1.5
-0.5
0.5
1.5
2.5
x (Å)

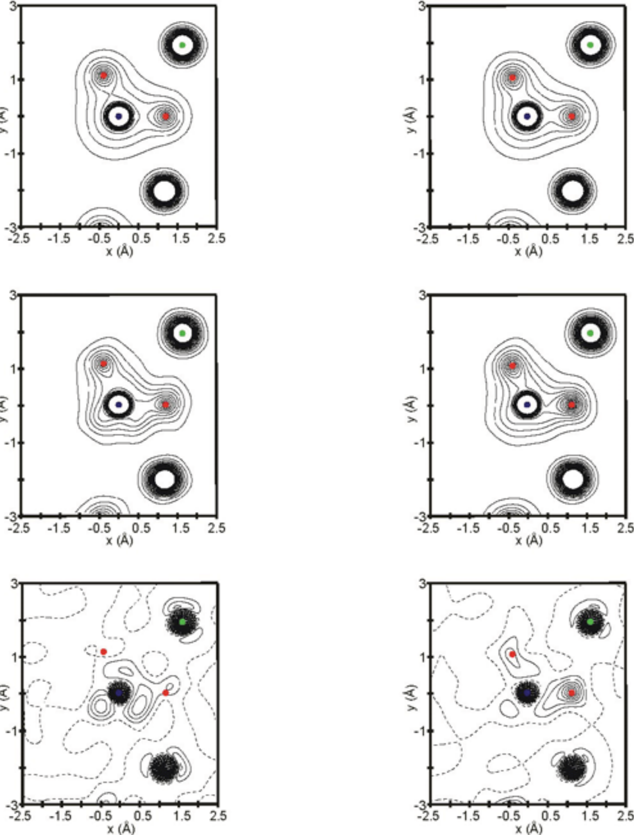
3
1
-1
-3
y (Å)
-2.5
-1.5
-0.5
0.5
1.5
2.5
x (Å)

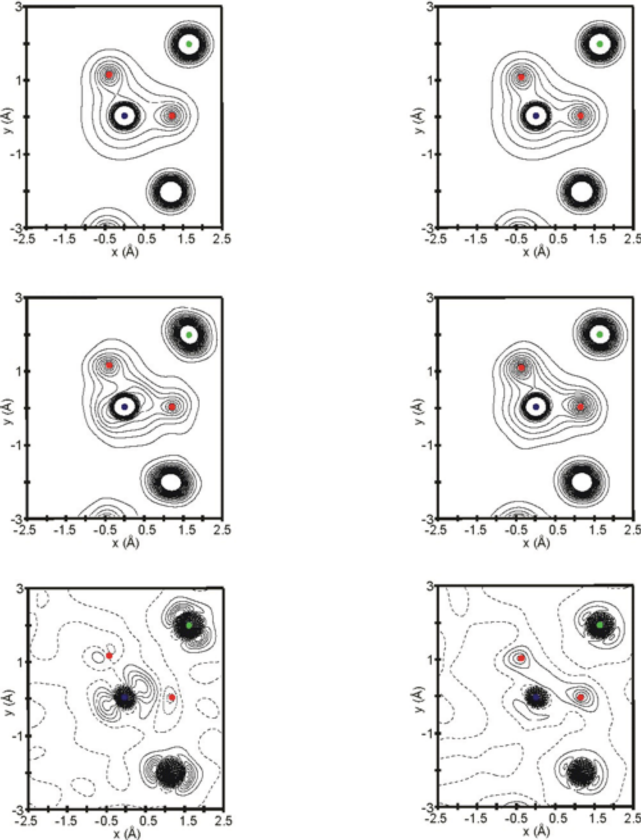
3
1
-1
-3
y (Å)
-2.5
-1.5
-0.5
0.5
1.5
2.5
x (Å)

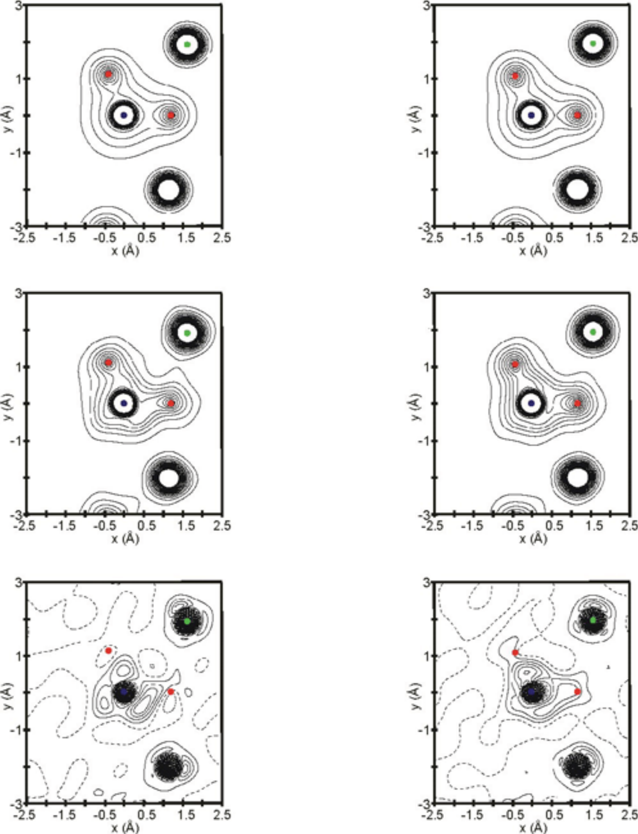
3
1
y (Å)
-1
-3
-2.5
-1.5
-0.5
0.5
1.5
2.5
x (Å)
3
1
y (Å)
-1
-3
-2.5
-1.5
-0.5
0.5
1.5
2.5
x (Å)
3
1
y (Å)
-1
-3
-2.5
-1.5
-0.5
0.5
1.5
2.5
x (Å)
3
1
y (Å)
-1
-3
-2.5
-1.5
-0.5
0.5
1.5
2.5
x (Å)
3
1
y (Å)
-1
-3
-2.5
-1.5
-0.5
0.5
1.5
2.5
x (Å)
3
1
y (Å)
-1
-3
-2.5
-1.5
-0.5
0.5
1.5
2.5
x (Å)

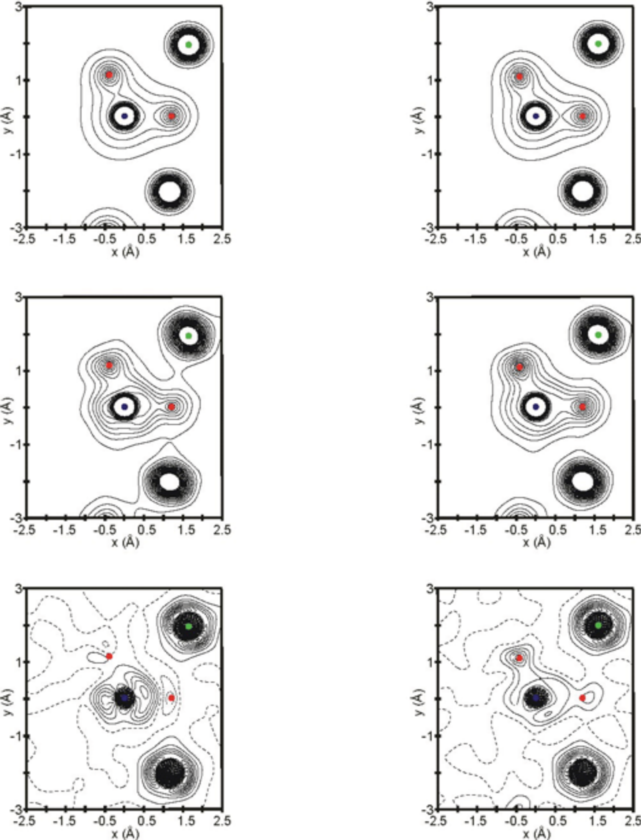
3
1
-1
-3
y (Å)
-2.5
-1.5
-0.5
0.5
1.5
2.5
x (Å)

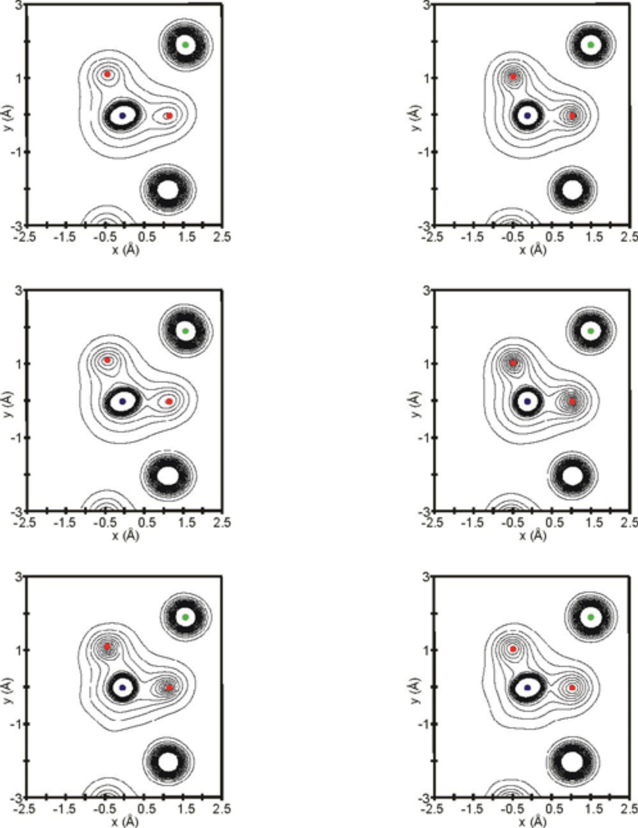
3
1
-1
-3
y (Å)
-2.5
-1.5
-0.5
0.5
1.5
2.5
x (Å)
3
1
-1
-3
y (Å)
-2.5
-1.5
-0.5
0.5
1.5
2.5
x (Å)
3
1
-1
-3
y (Å)
-2.5
-1.5
-0.5
0.5
1.5
2.5
x (Å)
3
1
-1
-3
y (Å)
-2.5
-1.5
-0.5
0.5
1.5
2.5
x (Å)
3
1
-1
-3
y (Å)
-2.5
-1.5
-0.5
0.5
1.5
2.5
x (Å)
3
1
-1
-3
y (Å)
-2.5
-1.5
-0.5
0.5
1.5
2.5
x (Å)

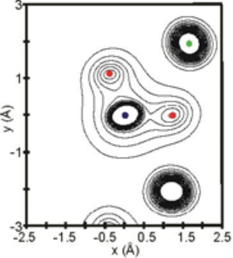
3
1
-1
-3
y (Å)
-2.5
-1.5
-0.5
0.5
1.5
2.5
x (Å)

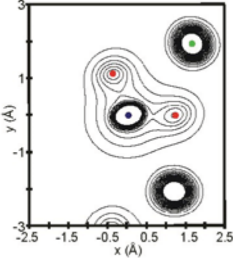
3
1
-1
-3
y (Å)
-2.5
-1.5
-0.5
0.5
1.5
2.5
x (Å)

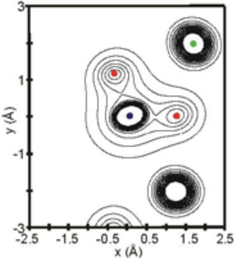
3
1
-1
-3
y (Å)
-2.5
-1.5
-0.5
0.5
1.5
2.5
x (Å)

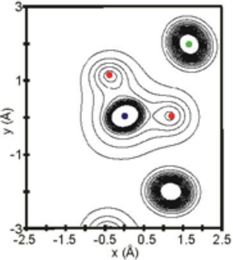
3
1
-1
-3
y (Å)
-2.5
-1.5
-0.5
0.5
1.5
2.5
x (Å)

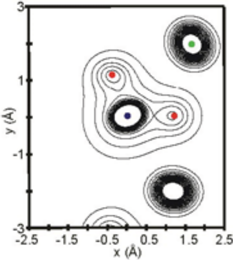
3
1
-1
-3
y (Å)
-2.5
-1.5
-0.5
0.5
1.5
2.5
x (Å)

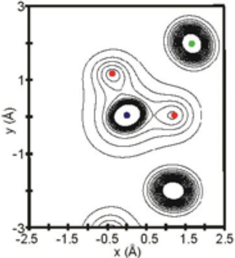
3
1
-1
-3
y (Å)
-2.5
-1.5
-0.5
0.5
1.5
2.5
x (Å)

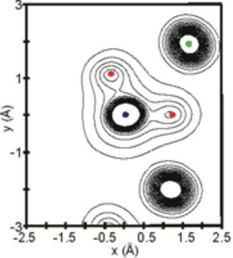
y (Å)
3
1
-1
-3
-2.5
-1.5
-0.5
0.5
1.5
2.5
x (Å)

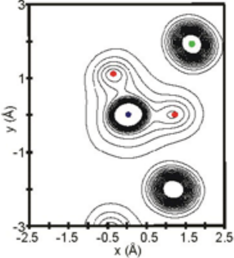
y (Å)
3
1
-1
-3
-2.5
-1.5
-0.5
0.5
1.5
2.5
x (Å)

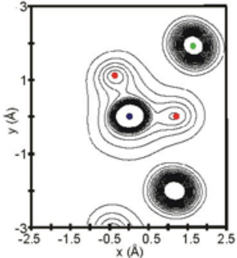
y (Å)
3
1
-1
-3
-2.5
-1.5
-0.5
0.5
1.5
2.5
x (Å)

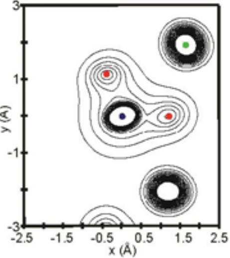
3
1
-1
-3
y (Å)
-2.5 -1.5 -0.5 0.5 1.5 2.5
x (Å)

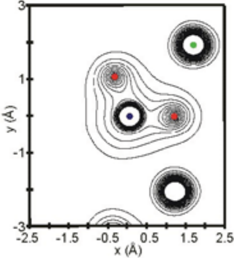
3
1
-1
-3
y (Å)
-2.5 -1.5 -0.5 0.5 1.5 2.5
x (Å)

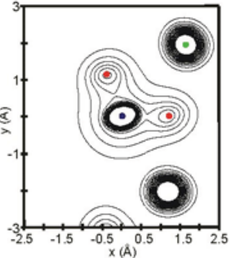
3
1
-1
-3
y (Å)
-2.5 -1.5 -0.5 0.5 1.5 2.5
x (Å)

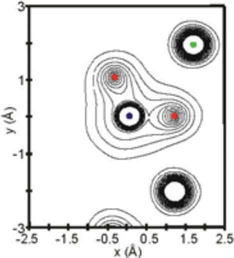
3
1
-1
-3
y (Å)
-2.5 -1.5 -0.5 0.5 1.5 2.5
x (Å)

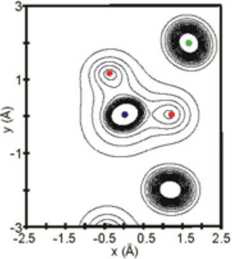
3
1
-1
-3
y (Å)
-2.5
-1.5
-0.5
0.5
1.5
2.5
x (Å)

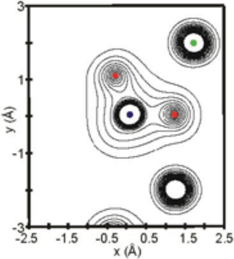
3
1
-1
-3
y (Å)
-2.5
-1.5
-0.5
0.5
1.5
2.5
x (Å)

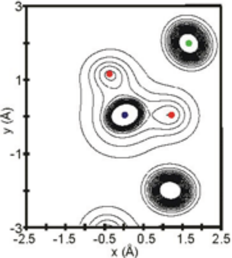
3
1
-1
-3
y (Å)
-2.5
-1.5
-0.5
0.5
1.5
2.5
x (Å)

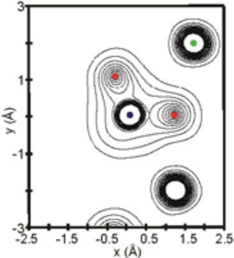
3
1
-1
-3
y (Å)
-2.5
-1.5
-0.5
0.5
1.5
2.5
x (Å)

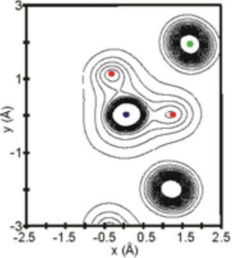
3
1
-1
-3
y (Å)
-2.5
-1.5
-0.5
0.5
1.5
2.5
x (Å)

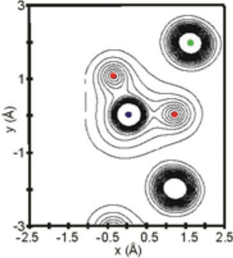
3
1
-1
-3
y (Å)
-2.5
-1.5
-0.5
0.5
1.5
2.5
x (Å)

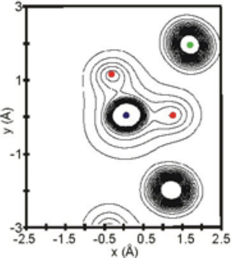
3
1
-1
-3
y (Å)
-2.5
-1.5
-0.5
0.5
1.5
2.5
x (Å)

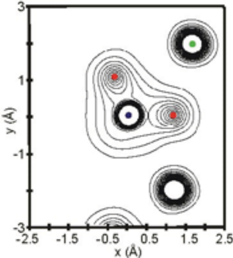
3
1
-1
-3
y (Å)
-2.5
-1.5
-0.5
0.5
1.5
2.5
x (Å)

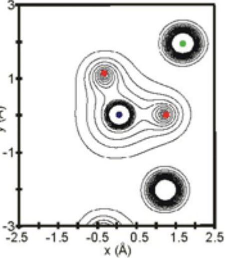
3
1
-1
-3
y (Å)
-2.5
-1.5
-0.5
0.5
1.5
2.5
x (Å)

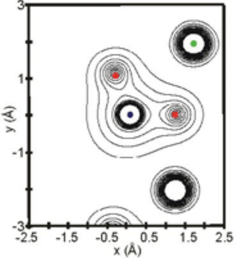
3
1
-1
-3
y (Å)
-2.5
-1.5
-0.5
0.5
1.5
2.5
x (Å)

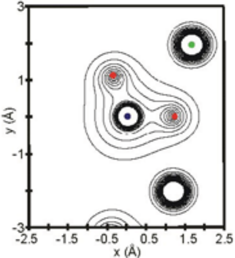
3
1
-1
-3
y (Å)
-2.5
-1.5
-0.5
0.5
1.5
2.5
x (Å)